University of Seville

Physics Degree 2014/2018

FEASIBILITY STUDY FOR A NEW IMAGING NEUTRAL PARTICLE ANALYSER IN THE ASDEX UPGRADE TOKAMAK

José Rueda Rueda

Supervisors:

Dr. Manuel García Muñoz

Dr. Eleonora Viezzer

Abstract

Magnetically confined fusion plasmas are the prior candidate to achieve an operative fusion power plant. The confinement of fast-ions, i.e. supra-thermal ions, is of paramount importance towards the development of a fully operative fusion reactor. To this end, knowledge of the complete distribution of fast-ions along the plasma is necessary.

During this bachelor thesis, a feasibility study for a new imaging neutral particle analyser (INPA) diagnostic at the ASDEX Upgrade tokamak was carried out. This detector is able to measure the energy and position of the fast-ion population with high resolution, contributing to the full understanding of its behaviour.

In this work, the necessary codes to obtain the synthetic signal, starting from the FIDASIM results, have been developed and tested. A sensitivity study of the geometry of the diagnostic and its impact on the resulting signal was carried out. For the final diagnostic position, the radial and energy resolutions have been estimated and show that the diagnostic can provide high resolution, both in energy (less than 6 keV) and radius (2 cm as lower limit).

Index

1 Introduction....1
2 Physics background....6
2.1 Motion of charged particles in an electromagnetic field....6
2.2 Charge-exchange reactions....9
2.3 Fast-ion generation....11
2.4 Neutral particles in a plasma....12
2.5 Birth distributions....13
3 Diagnostics....16
3.1 Fast-ion loss detector....16
3.2 Neutral particle analysers....19
3.3 Imaging neutral particle analyser....21
4 Numerical tools....24
4.1 FIDASIM....24
4.2 INPASIM....31
5 Results....34
5.1 Scintillator mapping and resolution study....34
5.2 Study of the synthetic signal....39
6 Conclusions and future work....43
Acknowledgements....44
Bibliography....45

1 Introduction

The increase in the world population goes hand in hand with an increase in the global energy demand. However, nowadays not the whole human population has access to the necessary amount of power. The production of energy all over the world is based on fossil fuels, which are limited, expensive and not homogeneously distributed, and pollution produced by them and other industrial activities are taking the planet to its limit.

Nuclear fusion energy, is a clean and virtually unlimited energy source. The term 'nuclear fusion' is used to name the physical process in which two or more nuclei merge into a new nucleus and other reaction products, for instance, neutrons or protons.

Depending on the mass of the involved nuclei, the reaction can be exothermic or endothermic. Thinking about energy production, only exothermic reactions are useful because only them release energy. There are several exothermic reactions, but just one is going to be presented here because is the one that have a greater cross-section in the range of temperatures that can be achieved in Earth, so it is the most appropriate reaction to develop a fusion reactor:

$$ {}^{2}_{1}D + {}^{3}_{1}T \rightarrow {}^{4}_{2}He + {}^{1}_{0}n + 17.6 \text{ MeV} \tag{1.1} $$

Although the cross-section of this reaction is still small (of the order of 10^{-27}m^2).

To develop an operating fusion reactor, the so called *ignition* must be fulfilled. The ignition is the situation where the energy that goes into the system (for example generated by fusion reactions) is equal that the energy expelled by the system. It can be shown, [1], that in order to achieve ignition, the following condition must be fulfilled:

$$nT\tau_E > 5 \cdot 10^{21} \text{ keVs/m}^3 \tag{1.2}$$

where n is the plasma density (particles per m^3), τ_E the energy confinement time and T the temperature. The temperature is given in keV. Along this bachelor thesis the temperature will be given in eV (or keV). The relation between the temperature in keV and the temperature in K is given by the Boltzmann constant: 1 eV is equal to 11605 K.

With the objective of fulfilling (1.2), two general approaches are followed: inertial confinement and magnetic confinement. In magnetic confinement fusion, two concepts exist: the tokamak[1] and the stellarator. Both of them are toroidal devices in which the matter is heated up to high temperatures; these temperatures must be high enough to be able to fulfil (1.2) without needing very long confinement times, (the normal operation temperature is on the order of keV), so most of the atoms are ionized and the system enters a plasma[2] state, the fourth state of matter. The idea of both devices is to achieve the confinement of the plasma by a strong magnetic field created by a set of toroidal coils since, as it will be shown in section 2.1, charged particles describe helicoidal trajectories along the magnetic field lines. In a purely toroidal field, due to the curvature of the field, particles are drifted depending on their charges and mass, this entail a charge separation which creates an electric field. This electric field, in combination with

1 The word tokamak is derived from Russian: 'toroidalnaya kamera and magnitnaya katushka'; meaning toroidal chamber and magnetic coil, [1].

2 In this work plasma will be understood as an ionized gas, globally neutral and characterized by collective effects.

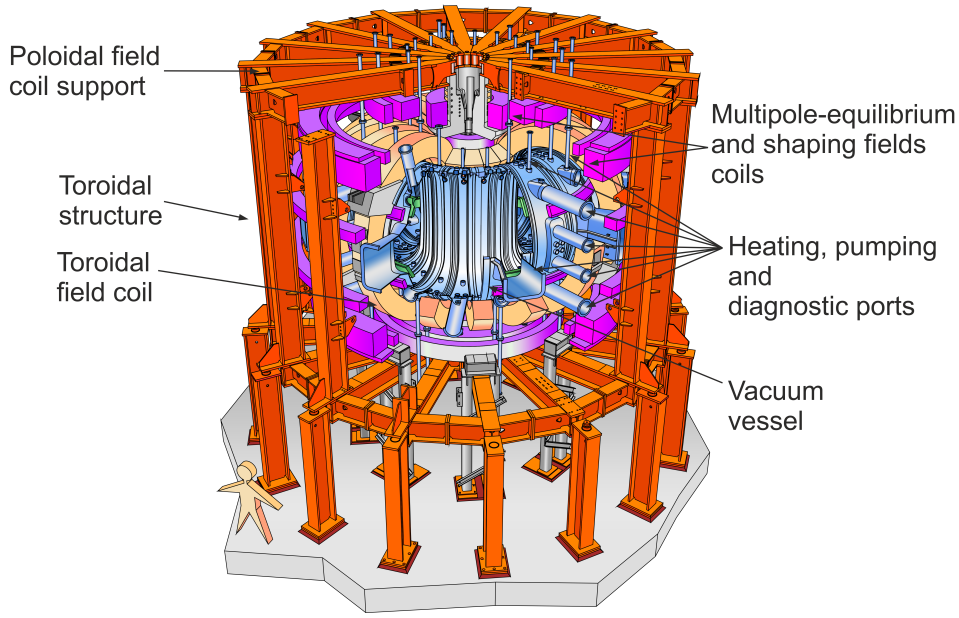

Figure 1.1: Overview of ASDEX Upgrade [2]

the toroidal magnetic field will cause a new drift, that will end in losses. In order to reduce these losses, a magnetic field perpendicular to the toroidal one is introduced that short-circuits the charge separation: tokamaks create this field by driving an electric current in the plasma using a transformer and stellarators by breaking the axial symmetry. In this work, only references to tokamaks will be done. Although the vertical component exist, the main component of the field is the toroidal one, ignoring borders effects, this fields is proportional to R^{-1}, where R is the distance from the axis of the torus. So the field is larger in the inner part of the torus and smaller in the outer one. The former is called high-field side (HFS) and the latter low-field side (LFS).

A schematic representation of ASDEX Upgrade (AUG)[3], on which this work was carried out, is shown in figure 1.1. The toroidal field coils are able to create a field of 3.2 T on the magnetic axis [2]. The various poloidal field coils are used to place and shape the plasma. Figure 1.1 also shows various ports used for diagnostics and heating systems as well as the vacuum vessel.

3 ASDEX stands for: Axial Symmetric Divertor EXperiment

In an operative fusion reactor, the vessel will be surrounded by a blanket which will have three main roles: first, it will shield the coils and other components; second it will absorb the energy expelled by the plasma and will transfer it to the auxiliary system that will transform it into electricity; third it will provide tritium for the reactor: one of the current concept is a lithium made blanked [3], tritium will be produced by reactions between neutrons created in (1.1) and lithium itself:

$$^{6}_{3}Li + ^{1}_{0}n \rightarrow ^{3}_{1}T + ^{4}_{2}He + 4.8\text{MeV} \tag{1.3}$$

$$^{7}_{3}Li + ^{1}_{0}n \rightarrow ^{3}_{1}T + ^{4}_{2}He + ^{1}_{0}n - 2.5\text{MeV} \tag{1.4}$$

The fuel in a fusion reactor consists of deuterium and tritium. Deuterium can be obtained from sea water; while, as it has been said, tritium is extracted from lithium, which is available in Earth's crust for $10,000$ of years; and will produce helium, a non-polluting gas. Furthermore, fusion power plants will not depend on climate characteristics to produce energy, so they can be installed all over the world and therefore construction and design costs will be reduced. Thus, fusion is the most promising energy source for the future.

As of yet, fusion reactors are still not functional and one of the reasons is the confinement of supra-thermal particles. This confinement is twofold: these particles need to spend enough time in the plasma to leave their energy in the system (by collisional processes); and a bad confinement implies the existence of a high energy flux of particles towards the reactor wall which, if localized, can cause structural damage.

The first step in the improvement of the confinement of these fast-ions is to obtain a full characterization of their distribution along the plasma and their response to perturbations. Many diagnostics, such as neutral particle analysers (NPA) [4] or fast-ion D-α (FIDA) spectrometers [5] have been used to study the confined fast-ion population. The fast-ion losses are measured with the fast-ion loss detector (FILD) that provides high-resolution measurements of their velocity space.

Nonetheless, a complete measurement of the fast-ion phase space distributions is necessary to be able to fully understand the transport mechanisms in order to acquire the capability to control them.

In this area, the detector developed in this bachelor thesis will make a significant contribution. The imaging neutral particle analyser (INPA) combines the already working concepts of the FILD and the NPA diagnostics to measure the radial position and energy of the fast-ion population. A detector of this type is already working in the DIII-D tokamak in San Diego and the first measurements obtained are promising [6].

In this bachelor thesis a feasibility study of the INPA diagnostic for the AUG tokamak is carried out. The codes to obtain a synthetic signal are presented, as well as the first order resolution study of the detector.

2 Physics background

In this chapter a brief overview of some important physical concepts is given. The movement of charged particles in electromagnetic field is presented, followed by and introduction to the charge-exchange reactions and generation of fast-ions and neutral particles; the chapter finishes with a brief description of the birth distributions.

Fusion plasmas have a density that make them difficult to study [7], they are not dense enough to neglect single particle motions and to describe the system with the ordinary fluid equations; but, they are so dense that only single particle trajectories can not be considered. Thus, single-particle movement and collective effects are necessary to explain the dynamics of the system. Nevertheless, for the objectives of this bachelor thesis, the single-particle description is appropriate to explain the operation of the diagnostic.

2.1 Motion of charged particles in an electromagnetic field

The movement of a single particle in an electromagnetic field is governed by the Lorentz force law:

$$m\frac{d\vec{v}}{dt} = q(\vec{E} + \vec{v} \times \vec{B}) \tag{2.1}$$

where m is the mass, $\vec{v}$ the velocity, q the charge of the particle and $\vec{E}, \vec{B}$ the electric and magnetic field.

To solve equation (2.1) a decomposition in velocity can be made: $\vec{v} = \vec{v}_{\parallel} + \vec{v}_{\perp}$, with $\vec{v}_{\parallel}$ and $\vec{v}_{\perp}$, respectively, the parallel and perpendicular components, referred to the magnetic field. With this, the equations of motion become:

$$\begin{cases} m\dfrac{d\vec{v}_{\parallel}}{dt} = q\vec{E}_{\parallel} \\ m\dfrac{d\vec{v}_{\perp}}{dt} = q(\vec{E}_{\perp} + \vec{v}_{\perp} \times \vec{B}) \end{cases} \tag{2.2}$$

The solution of (2.2) is straight forward if the fields are considered static and homogeneous. The first equation would let to an uniformly accelerated motion. For the second equation, the solution would be a periodic circular motion, induced by the magnetic field, superposed to a drift, induced by the electric field. The radius, r_L (Larmor radius) and frequency, ω_L (Larmor frequency) of the circular motion are:

$$r_L = \frac{mv_{\perp}}{|q|B} \tag{2.3}$$

$$\omega_L = \frac{qB}{m} \tag{2.4}$$

Notice that ω_L can be positive or negative, depending on the sign of the charge. This will define the direction of the gyromotion, left-handed or right-handed referred to the magnetic field.

The average of the second equation of (2.2) over one gyroperiod is:

$$\left\langle m\frac{\vec{v}_{\perp}}{dt} \right\rangle = 0 = q(\vec{E}_{\perp} + \langle\vec{v}_{\perp}\rangle \times \vec{B}) \tag{2.5}$$

Multiplying equation (2.5) by $\vec{B}$ results in:

$$\langle v_{\perp}\rangle = \frac{\vec{E} \times \vec{B}}{B^2} \tag{2.6}$$

Equation (2.6) is called $\vec{E} \times \vec{B}$ drift.

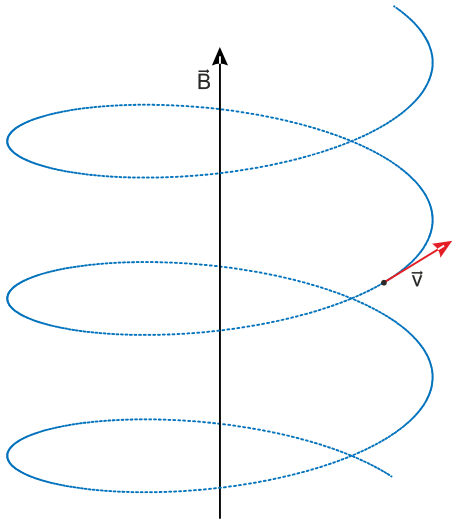

Figure 2.1: Trajectory of a charged particle in an electromagnetic field. The electric field is supposed to be zero.

If the drift is negligible or $\vec{E}$ is parallel to $\vec{B}$, the composition of the perpendicular and parallel movement will let to an helicoidal trajectory with the axis along the magnetic field line. An example of this is represented in figure 2.1

If the general case is considered, where the fields are not static nor homogeneous, the same decomposition of the movement in a circular motion and a drift can be made if $(\nabla\vec{B})/B$ is large with respect to r_L and $(\frac{\partial\vec{B}}{\partial t})/B$ is small compared to ω_L, [1]. Any force can cause the drift motion, but in a tokamak the most important drifts to consider are the already mentioned $\vec{E}\times\vec{B}$ drift, the ∇B drift $(-\frac{mv_\perp^2}{2qB^3}\nabla B\times\vec{B})$ that arises due to the fact that the $\vec{B}$ field is not homogeneous, and the curvature drift $(-\frac{mv_\parallel^2}{qB^3}\nabla B\times\vec{B})$ results from the centrifugal force.

Although this approach to the solution of the trajectory is formally valid, it is not the set of variables that are usually chosen to describe the phase space of plasma particles inside a tokamak. In a tokamak the dimensions of the problem are reduced due to the toroidal symmetry and the magnetic moment. It is clear that the first one directly reduces the dimension, the second one is more subtle: the

magnetic moment of a particle inside a tokamak is an adiabatic invariant. The last statement is true if the variations of the magnetic field are slower compared with the gyromotion of the particle, the same assumption to decompose the movement in a gyromotion plus a drift. The magnetic moment of a particle is defined as:

$$\mu = \frac{\frac{1}{2}mv_{\perp}^2}{B} \tag{2.7}$$

Hence, to describe the phase space of the particle only four parameters are needed. The position is usually described with the major radius, R, distance to the torus axis of the tokamak, and z, height above the midplane of the system. The velocity is usually referred to the kinetic energy and the pitch angle. There are various definitions of the latter, in this work will be used:

$$p \equiv -\frac{v_{\parallel}}{v} \tag{2.8}$$

pitch and *pitch angle* will be considered as equivalent terms, given by equation (2.8).

2.2 Charge-exchange reactions

Charge-exchange reactions (CX) are the physical mechanisms behind the signal of many diagnostics, for instance, the NPA, FIDA and INPA. They are interactions between an ion and a neutral particle in which an electron from the neutral is transferred to the ion. If the neutral is considered to be deuterium the reaction would be written as:

$$D^0 + A^{Z+} \rightarrow D^+ + A^{*(Z-1)+} \tag{2.9}$$

If the ion A is considered to be deuterium, the equation (2.9) would read as:

$$D^0 + D^+ \rightarrow D^+ + D^{*0} \tag{2.10}$$

In these reactions only the electron is transferred, no momentum or energy is exchanged (actually, a small amount of energy is exchanged and there will be a small change of momentum but both of them are negligible compared to the initial

ones). As there is no significant momentum exchange, there is no scattering, so the new neutral carries on all the mechanical information about the old ion. Hence, measuring the properties of this neutral, which can escape from the plasma as it is not confined by the magnetic field, gives directly information about the confined fast-ion population.

The new ion is born in an excited state. The decay from this state is the source of the FIDA diagnostic. The energy of these emissions are much smaller than the energy of the neutral (the electronic levels of the deuterium are essentially the same of the ones of the hydrogen, so the energy of the emissions is in the order of the eV); therefore, it is assumed that the neutral has all the energy of the ion.

There are several processes that compete with CX reactions; for instance: electron-impact ionization and ion-impact ionization. A comparison of the cross-sections of the three reactions is shown in figure 2.2. As can be seen, the CX reaction is the dominant mechanism at low energies and even in the range of tens of keV.

A graphical representation of the process can be seen in figure 2.3. It must be pointed out that the new neutral carries on the full velocity of the old ion, not only the one of its gyrocenter, so there is no predominant direction for the emission

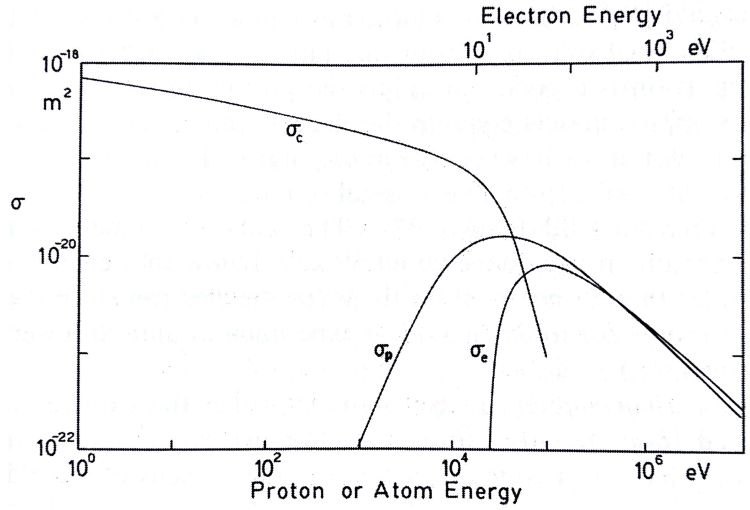

Figure 2.2: Cross-sections for electron-impact ionization, σ_e, ion-impact ionization, σ_p, and charge exchange, σ_C [8].

of the neutral particle. As all detectors have a finite size, not all the created neutrals can be recorded.

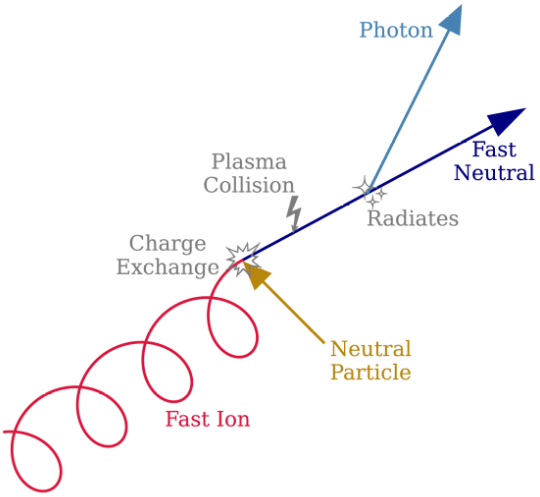

Figure 2.3: Graphical scheme of the CX process, [9].

2.3 Fast-ion generation

Fast-ions are charged particles whose kinetic energy is bigger than the average kinetic energy. They can be generated by the nuclear reactions or by external sources. Using external heating sources there are two main ways to create fast-ions in the plasma: by a neutral beam injector (NBI) or by ion cyclotron resonance heating (ICRH).

NBIs are small accelerators connected to the tokamak torus. They accelerate ions, H^+ or D^+, depending on the set up, with a difference of potential (at AUG 72 kV for hydrogen and 93 kV for deuterium in one of the beam lines and 55 kV and 60 kV in the other one [2]) and then these ions are neutralized with a gas target and are injected into the plasma. As these neutral particles enter the plasma, they suffer collisions with electrons and ions and CX processes which lead to their ionization, and they become part of the fast-ion plasma population. A key

aspect of the NBI injection is that not only particles with one energy are injected in the plasma. Not only H^+ or D^+ are created, but H_2^+, H_3^+, D_2^+ and D_3^+, respectively, are created as well. These molecules are accelerated to the same potential, so they gain the same kinetic energy; however in the neutraliser they dissociate and the energy is divided between the atoms, so particles with half and third of energy are injected.

Ion cyclotron resonance heating is the other mechanism to create fast-ion, in this case, no particles are injected in the tokamak, but electromagnetic waves are used. Due to the plasma dielectric response not all frequencies can propagate in the system, there are gaps of them which are reflected, [10]. Three ranges of frequencies can be used [11]: ion cyclotron frequency (30-80MHz), the so-called lower hybrid frequency (several GHz) and electron cyclotron frequency (several tens of GHz). The ion cyclotron resonance heating use the first one. The absorption of energy by the ions is due to resonance between the particle gyromotion and the wave.

2.4 Neutral particles in a plasma

Neutral particles can exist in the plasma. There is an already mentioned source of these particles: the NBI provides the plasma with an important number of them; but other possible source of neutral particles exists. Due to electron impact, hydrogen molecules released by the wall can dissociate following the reaction, [1]:

$$H_2^0 + e^- \rightarrow H^0 + H^0 + e^- \tag{2.11}$$

These neutral particles do not follow the magnetic field lines and can escape the plasma; but there is a probability of these particles to suffer a CX reaction with an ion of the plasma, so a new neutral is created. New CX reactions and neutral production can continue as long as CX reactions have a higher probability than ionizations.

Other mechanism, such as charge recombination, are sources of neutral particles, but they are usually less important processes because their production rates are smaller [1].

In the signal analysis a distinction can be made between the neutral particles depending on their birth characteristics: the ones coming from the interaction with the NBI will be called active and the rest will be called passive.

Another important concept is the beam halo [5]. The halo is the cloud of neutrals particle surrounding the NBI ray. It is formed by collisional processes only a few microseconds after the NBI is switched on. These neutrals can propagate perpendicular to the NBI path, so the distribution of neutrals in the halo is relatively wide and can give a significant contribution to the measured signal; although the mean free path of these particles is only a few centimetres.

2.5 Birth distributions

The distribution of the fast-ions created as the result of the interaction between the plasma and the NBI will be denoted in this work as *birth distribution*. Its study exceeds the objectives of this bachelor thesis but there are two facts about it that are fundamental for the diagnostic.

When the NBI is switched on, a flux of high energy neutrals is injected into the plasma. As mentioned in section 2.3, these neutral particles suffer a CX reaction and become the new fast-ions with the same velocity that they carried on. This velocity has its direction determined by the injection geometry and its modulus fixed by the injection energy.

In each point along the NBI path, where CX can occur, the magnetic field lines form a fixed angle with the injection line, as it is shown in figure 2.4, so the possible pitch angles that the new ion can have are fixed by the geometry and will be characteristic of the radial birth position. An example of the birth profile of

NBI3 is shown in figure 2.5. As shown, neutrals with an energy of 20 keV have a smaller range of pitch. This is due to its penetration in the plasma, as they have less energy, they travel less distance so a smaller range of pitch can be populated. In contrast, particles with an energy of 60 keV penetrate a longer distance in the plasma, so a bigger range of pitch can be populated.

The deposition profiles are related to penetration of the beam into the plasma. Processes such as ionization and CX take place so the number of neutrals that are deposited near the inner radius is smaller than the one deposited at the outer zone.

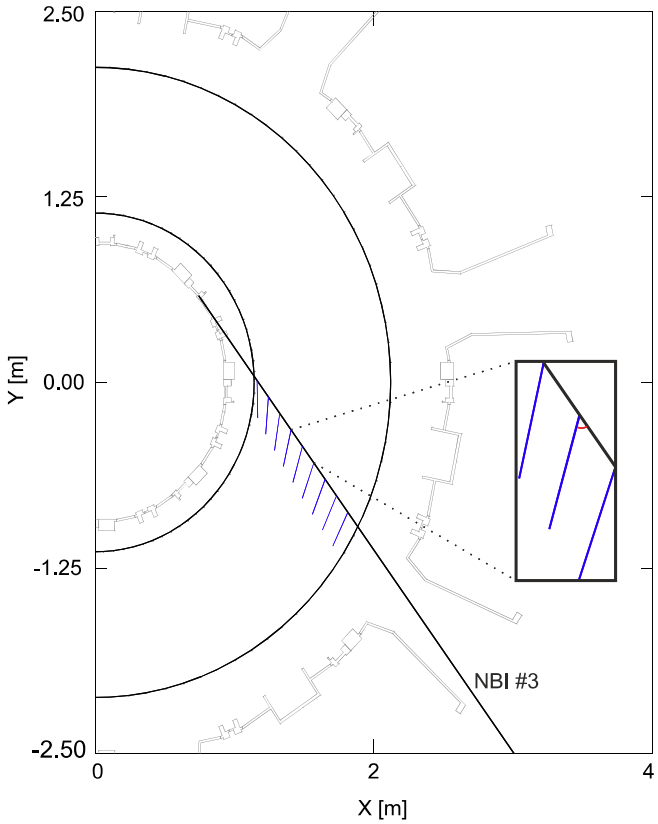

Figure 2.4: NBI source #3 (solid black line) and total magnetic field lines at different point of it (blue lines). In the subplot, a zoom of a part of the NBI beam is presented with the angle between the magnetic field lines and the NBI beam highlighted in red.

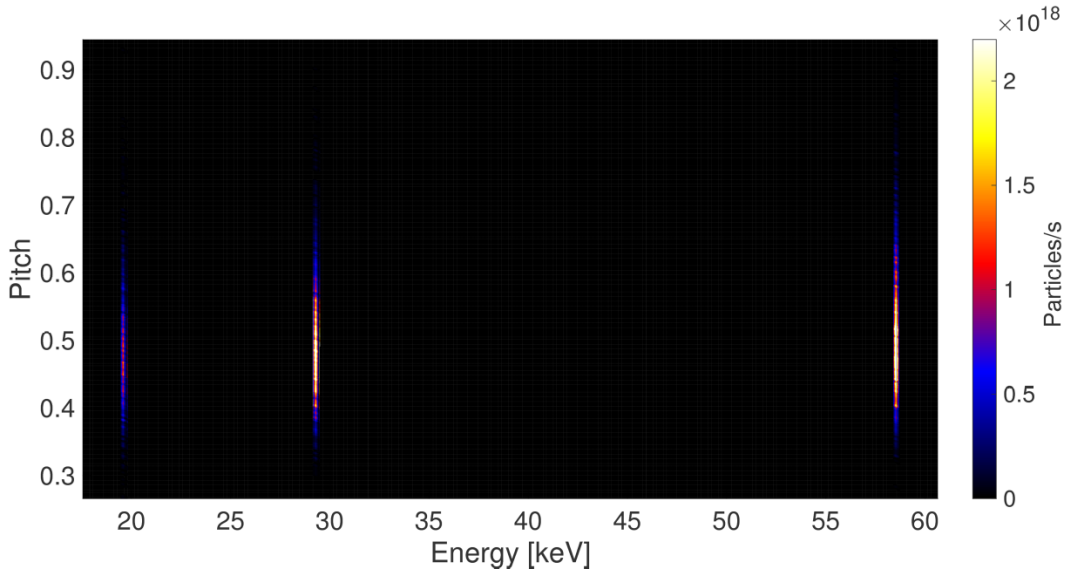

Figure 2.5: Birth profile of NBI beam 3 calculated with FIDASIM. The larger energy component has a bigger range of pitch because it penetrates more in the plasma.

The calculations of the radial deposition profiles simulated with FIDASIM are shown in figure 2.6. As shown, the three profiles have a maximum at the outer radius of the plasma so in this region active neutral population is lager. The INPA will rely on CX processes with neutral particles so the signal coming from this region will be larger in magnitude that the signal coming from the inner parts of the plasma.

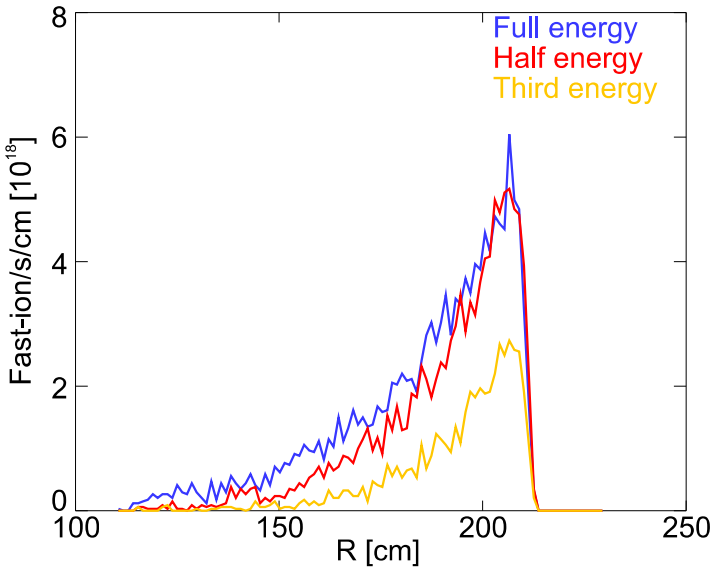

Figure 2.6: Radial birth profile of NBI 3 calculated with FIDASIM.

3 Diagnostics

In this chapter, the basic concepts of fast-ion loss detector (FILD) and neutral particle analyser (NPA) will be presented, in order to introduce the relevant concepts to understand the imaging neutral particle analyser (INPA). The main aspects of the INPA are introduced.

3.1 Fast-ion loss detector

FILDs installed at AUG [12] are scintillator based diagnostics designed to measure fast-ion losses with high resolution in time, energy and pitch. The mass and the charge of the incident ion are not resolved. The detector consists of a probe located near the plasma edge. Its main elements are a graphite cup protection (that allows the system to survive the high heat load), a collimator and a scintillator.

Basically, the measurement process can be schematized as follows:

- Ions in the plasma are expelled from the plasma due to drift motions, caused by magnetohydrodynamic (MHD) instabilities or any other mechanism.
- Some of them will eventually reach the detector pinhole and go through the collimator.

- If the pitch and energy of the particles are inside the range allowed by the collimator they will enter the scintillator chamber, where the local magnetic field of the tokamak serves as a spectrometer: ions will gyrate along the magnetic field lines on helicoidal trajectories (magnetic field can be considered as constant in the small region near the scintillator). The gyroradius of this movement will be given by their perpendicular velocity and magnetic field (equation (2.3)) and the uniform movement along $\vec{B}$-lines will be given by their parallel velocity so the collision point on the scintillator can be expressed as function on their energy and pitch. In the collision point, light is emitted due to excitation processes in the scintillator material.
- The emitted light is detected with two systems. One of them is a charge-coupled device (CCD) camera which provides good velocity space resolution and the other one, for instance, an avalanche photodiode (APD), provides a good temporal resolution.

A CAD design of the detector and a scheme of its working process can be seen in figure 3.1. The collimator is designed together with the pinhole: their shape and size will determine the resolution of the system, the range of energy and pitch that can be measured and the collimator factor, defined as the ratio of particles blocked by the collimator.

The scintillator is the fundamental part of this detector performance, similar as for the INPA. The general requirements of the scintillator material are, [12], [13]: having good sensitivity to the particles of interest (fast-ions) and low sensitivity to the others; emitting light in the operation range of temperatures (400-700K) and having fast response and high saturation levels. TG-Green ($SrGa_2S_4 : Eu^{2+}$) is used in the FILD systems installed at AUG and is the most promising candidate to

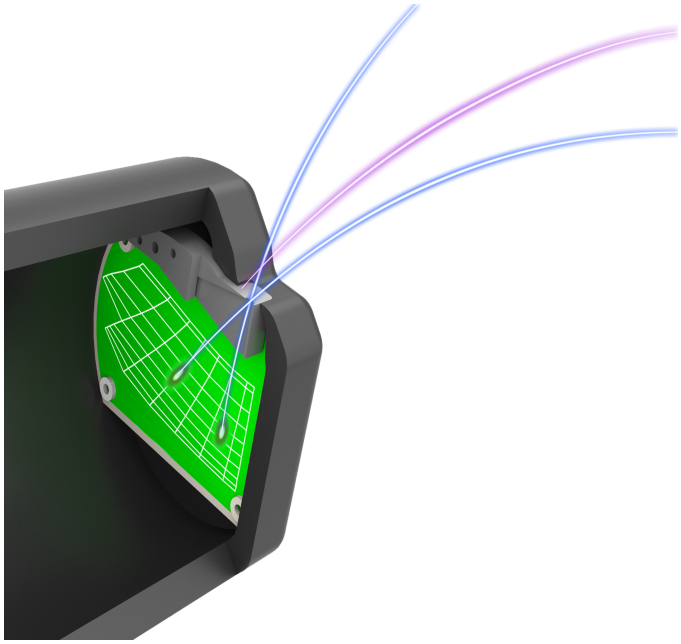

Figure 3.1: CAD view of the detector head, the scintillator and collimator. Typical ion trajectories are also shown. Note that the purple trajectory is blocked by the collimator.

be used in the INPA diagnostic. A full description of this scintillator material and other candidates can be found in [14], [15].

As mentioned before, the impact point of an ion on the scintillator depends on its energy and pitch; finding the relation between these elements is known as mapping. The FILDSIM code [16] is used for the mapping: it launches random markers in the pinhole with pitch and gyroradius inside a prefixed range and with a random gyrophase, then it tracks them until they collide with the collimator or the scintillator. It stores the collision point at the scintillator of all the ions and calculates the centroid of the collision point distribution of each pair gyroradius-pitch. With all of these centroids, the grid of the scintillator map is defined.

Recent advances in the mechanical system of the FILD diagnostic which allows the orientation the detector without opening the tokamak [17] and even absolute measurement of fast-ion flux have been made [15], [16].

3.2 Neutral particle analysers

NPAs are one of the first diagnostics that were implemented to measure the properties of fast-ions [18]. There are many types of NPA systems, each one with its advantages and disadvantages, but all of them are based on the same CX reaction, presented in section 2.2 and all of them can be schematized as aperture that controls the incident particle flux, a collimator and a counting system. The measurement principle of the diagnostic is as follows:

- An ion of the plasma suffers a CX process and becomes a neutral particle. As it is not confined any more by the magnetic field, it travels straight on through the plasma. If it does not suffer a collision that entails its ionization, the particle exits the plasma.
- If its velocity and position are inside the range accepted by the pinhole and collimator, the neutral goes inside the detector.
- Once the neutral is in the detector, depending on the type of NPA a variety of physical processes can happen:
  - $\vec{E} \times \vec{B}$ spectrometers: the neutral travels through a collimator, suffers an ionization and enters a region with fixed $\vec{E}, \vec{B}$ fields, where it is deflected according to its mass, charge and energy. A series of multichannels record the signal. Further information about these NPAs can be found in [18].

    These systems offer the possibility of mass separation, and thus allows information on the species mix that form the fast-ion population. However, these detectors do not use the local magnetic field of the tokamak, they are located out of the vessel and use an external electromagnetic field. This field is much smaller so the gyroradii are bigger. In the end, this detector has a size that makes the exploration

of different plasma regions complicated (they are fixed to almost only one line of sight (LOS)).

- Solid state NPA (ssNPA): the neutral is counted by a fast AXUV diode which generates a charge pulse that is processed by an electronic chain. The height of the pulse is proportional to the energy of the incident neutral, which gives the detector the capability of measuring the energy distribution of the neutrals.

  These systems have a small size, so they can be oriented to explore a large range of LOS; nevertheless, the possibility of isotope separation is lost because the system only measure the energy of the incident particle and in the case of the installed system at AUG the count rate is limited to 140kcps due to the data acquisition system, [4].

A LOS is the straight line defined by the position of the detector head and the measurement location (probe volume). Some diagnostics like the ssNPA only explore one LOS and others, such as FIDA, have several LOSs.

For the ssNPA diagnostic, the geometry of the LOS defines the possible pitch that can be measured. If a diagnostic with perfect collimation, i.e. only particles with velocity along the LOS can reach the detector, is assumed, then, as LOS will intercept the magnetic lines at given angles, different depending on the position inside the plasma, the range of pitch that can be explored is limited. In figure 3.2, the LOS explored by the ssNPA installed at AUG and the magnetic field lines in some points along it are shown. In this case, the range of pitch that can be explored is relatively small, so only a small region of the phase space of the fast-ions can be explored.

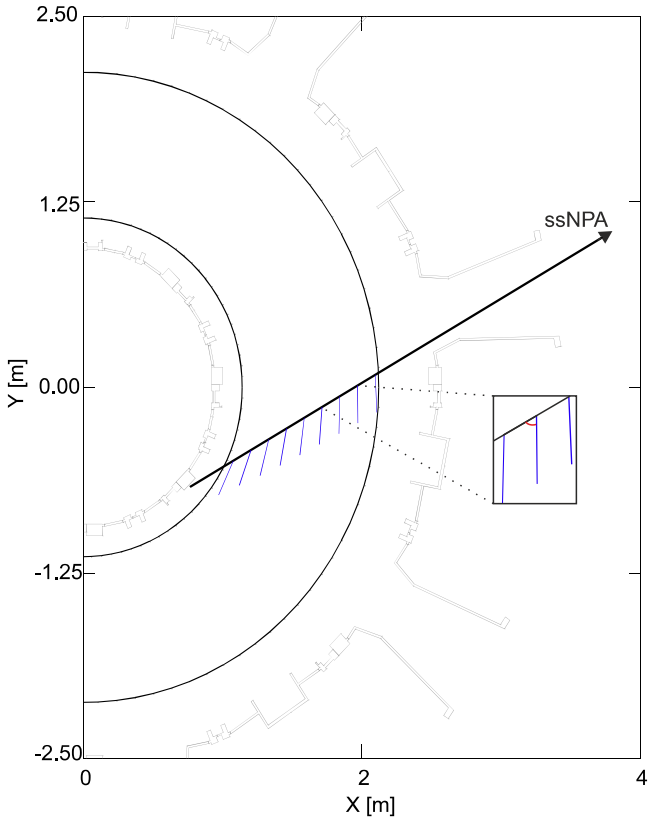

Figure 3.2: LOS (solid black line) and magnetic field (blue lines). The geometry of the LOS defines the angles between the LOS and the B field (highlighted in red in the subplot). Only particles with given pitch can reach the detector.

3.3 Imaging neutral particle analyser

The INPA [6] measures the energy and radial position of the fast-ions combining the already working measuring principles of FILD and NPA systems. The INPA diagnostic measures the energy and pitch of the outgoing neutral flux after the CX processes in the plasma. As mentioned in section 2.2, the energy of these neutrals is the energy of the ions that took part in the CX reactions. The capability to resolve the radial position is based on the correlation between pitch and LOS.

The INPA is similar to the already mentioned $\vec{E} \times \vec{B}$-NPA (see section 3.2), it collimates the incident particle flux, ionizes it and uses a magnetic field as a

spectrometer. As the standard NPA systems, the INPA is a line integrated diagnostic i.e. the recorded signal from each LOS corresponds to the sum of all CX processes over the full LOS. The fundamental difference to the $\vec{E} \times \vec{B}$-NPA is that the INPA uses a thin carbon foil as ionizer and the local magnetic field in the tokamak as spectrometer; so, the measured gyroradii are much smaller, the detector is compact and it can be orientated to cover the range of LOS desirable for the study.

To characterize the effect of the carbon foil, SRIM[4] [19] simulations have been performed. These simulations have demonstrated that the scattering induced by the carbon foil is negligible and the energy losses are small. The calculated energy losses for deuterium in a 10 nm carbon foil are shown in figure 3.3. The energy loss is small and as first approximation this effect could even be ignored.

To measure the ionized particles the INPA uses as scintillator plate, like the FILD diagnostic installed at AUG does [12], so the capability to resolve the isotope mass is lost; although using the scintillator plate the diagnostic has the same time resolution of FILD, 1 MHz [20] . A schematic overview of the diagnostic is shown in figure 3.4.

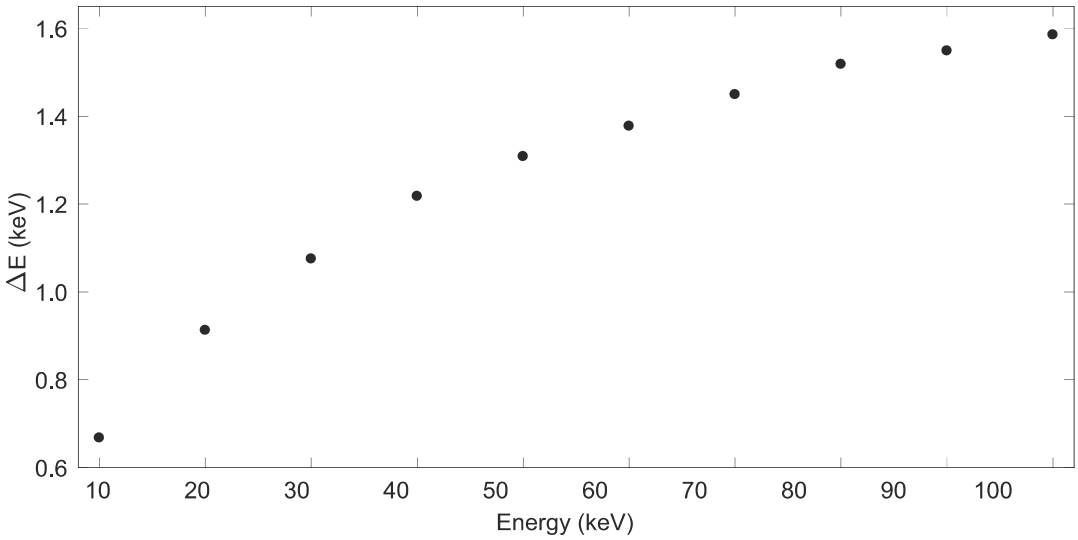

Figure 3.3: SRIM simulations for the energy loss of deuterium in a 10 nm carbon foil.

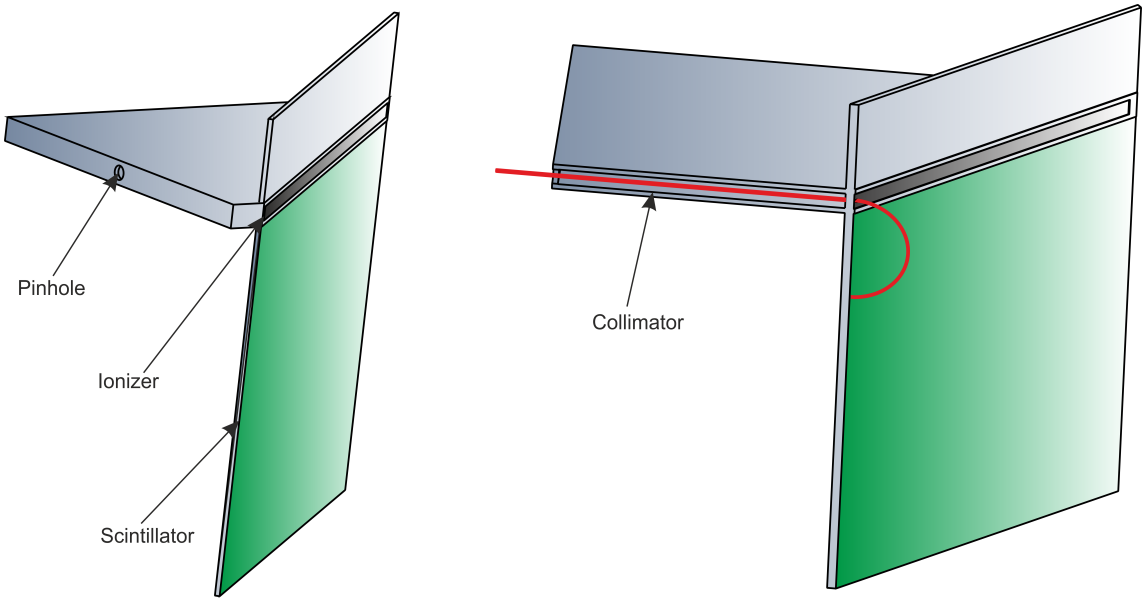

Figure 3.4: Left figure: Schematic 3D model of the INPA. Right figure: vertical cut of the 3D view. A particle trajectory can be seen highlighted in red.

In contrast to the ssNPA, the INPA allows the measurement of a relatively broad region of the phase-space because several LOSs are measured simultaneously. The range of LOSs that can be explored is determinate by the collimator. A representation of the LOSs explored is shown in figure 3.5.

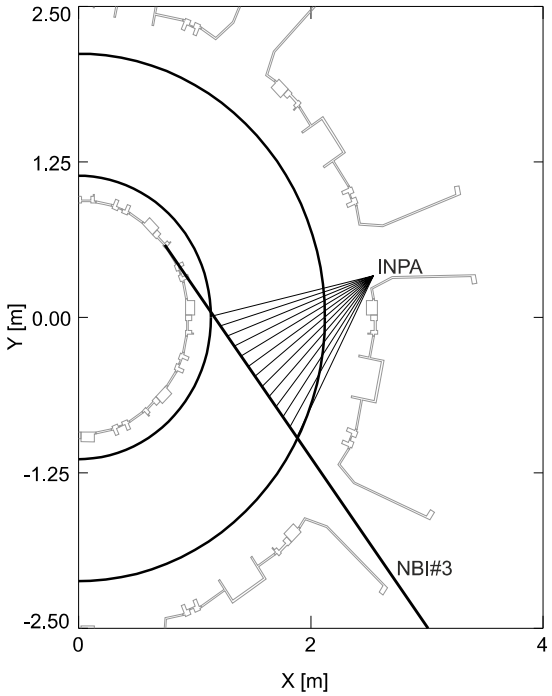

Figure 3.5: LOS explored by the INPA in its simulated detector position.

4 Numerical tools

In this section the two simulation codes used during the work are presented. The first one, FIDASIM [21] [5], has been used to compute the neutral flux that reaches the detector. The second one, INPASIM, has been developed during this work based on some routines of FILDSIM, [16]. The main part of the INPASIM code has been programmed in FORTRAN95, the pre- and post-processing sections have been programmed in MATLAB©.

4.1 FIDASIM

FIDASIM uses the geometry of the system (diagnostic and NBI), the equilibrium profiles, densities, temperatures, effective charge (Z_{eff})[5] and toroidal rotation[6] as an input. In addition, the electric and magnetic fields, the fast-ion distribution function and numerical parameters such as grid spacing and number of markers to simulate are provided. Once the inputs are loaded, the integration mesh is created and all inputs are mapped onto it. Then, the neutral density calculation following a Monte Carlo approach is performed. Finally, two sections that are independent of each other are used to calculate the FIDA and NPA signals.

5 Z_{eff} is defined as $Z_{eff} = \frac{\sum_i n_i Z_i^2}{n_e}$ where n_i, Z_i denotes ions density and charge and n_e denote electron density.

6 Toroidal rotation refers to the velocity of the plasma in the toroidal direction.

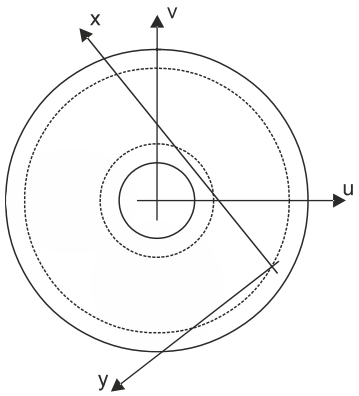

Figure 4.1: Coordinate systems used by FIDASIM.

4.1.1 Overview of inputs

During the execution, FIDASIM uses two coordinate systems: one of them is the torus system {u,v,z}, in which all the geometries are defined, and a second one, with the x-axis along the NBI path and with the origin just outside the plasma, in which all the calculations are done. An illustration of these two system is shown in figure 4.1. With them, the Cartesian integration grid is defined by its limits and number of cells in the three dimensions of space.

The NBI is defined by its geometry (position, width and height), divergence, power and species mix. All parameters are read from the AUG shot file[7] system.

To define the diagnostic, four elements can be modified:

1. Type of diagnostic: NPA or FIDA
2. Detector head: simulated as a circular pinhole perpendicular to the LOS and centred in a position $\vec{c}$. The $\vec{c}$ vector and the radius of the pinhole must be given to the program.
3. LOS: defined by its two ends, one of them is the already defined detector head position ($\vec{c}$), so only a new point must be given to the program.

7 Each discharge in AUG is called shot. The shot file system is an internal network service that contains information about all parameters of the discharges.

4. Opening angle. This variable will define a limit for the markers to be counted. Only markers with a velocity that make an angle (with respect to the LOS) equal or smaller to the opening angle are counted as signal for the diagnostic.

During this work, a radius of 3 mm has been chosen to simulate the detector pinhole, similar to the DIII-D configuration, [6]. The head position, $\vec{c}$, has been placed such that the LOSs explored by the diagnostic cover the NBI beam 3, with the appropriate angle to be able to explore the pitch injection range of NBI beam 8. Although this condition has been matched at the high field side, as will be seen in chapter 5 this will lead to a smaller signal.

The last elements of the input structure are the plasma parameters and profiles. All parameters of the plasma equilibrium such as the electron and ion temperatures and densities, Z_{eff} and the toroidal rotation are taken from TRANSP[8] simulations. All profiles are measured with specific diagnostics and the fit to the profiles are used as input for TRANSP.

The fast-ion distribution function and the thermal neutral distribution are important for the calculations. The former is important for the selection of the geometry and the latter is key for the passive signal. An example of the fast-ion distribution function used in this bachelor thesis is shown in figure 4.3. This distribution function is a slowing down distribution (the distribution of fast-ions when they have been in the plasma during a certain time such that collisional processes have created a spreading in the pitch. Note that this spreading only occurs at low energies. This is due to the collision cross-sections: at high energies collisions with electrons are dominant so no scattering occurs, at low energy the dominant ones are collisions with ions, thus scattering is important). The distribution has been calculated with TRANSP and set up for shot #30585. In this

8 TRANSP is a transport code which predicts neutron rates, energy confinement times and fast-ion distribution functions, amongst others.

discharge, NBI beam 8 and 3 were switched on and density and temperatures were in the usual range of fast-ion experiments. This can be seen in figure 4.2. This representation serves as an example to explain the typical coordinate system in tokamak physics: the normalized toroidal flux coordinate, ρ_t, according to the magnetic flux surfaces. A magnetic flux surface is a surface whose normal vector is perpendicular to the magnetic field, so the magnetic flux traversing a magnetic field surface is zero. The normalized toroidal flux coordinate is defined as [22] :

$$\rho_t = \sqrt{\frac{\Phi - \Phi_0}{\Phi_s - \Phi_0}} \tag{4.1}$$

where Φ is the toroidal flux enclosed within the flux surface, Φ_0 is the toroidal magnetic flux at the magnetic axis and Φ_s is the toroidal flux enclosed by the separatrix. The separatrix is the last closed magnetic flux surface.

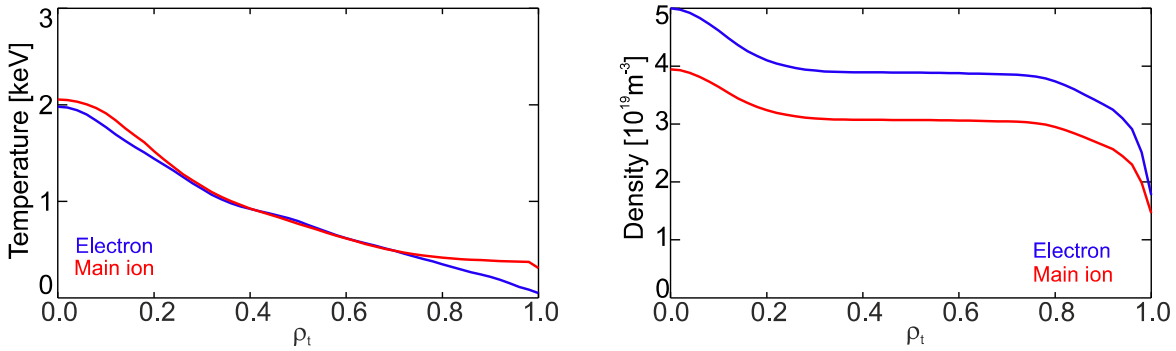

Figure 4.2: Temperature and density profiles used in the simulations during this bachelor thesis.

In figure 4.4 the passive neutral distribution as a function of the normalized radius can be seen. This profile has been defined parametrically taking into account the expected order of magnitude of the passive neutrals and the expected shapes of the density, i.e., maximum at the edge and minimum at the plasma centre. This is in agreement with the one exposed in [23].

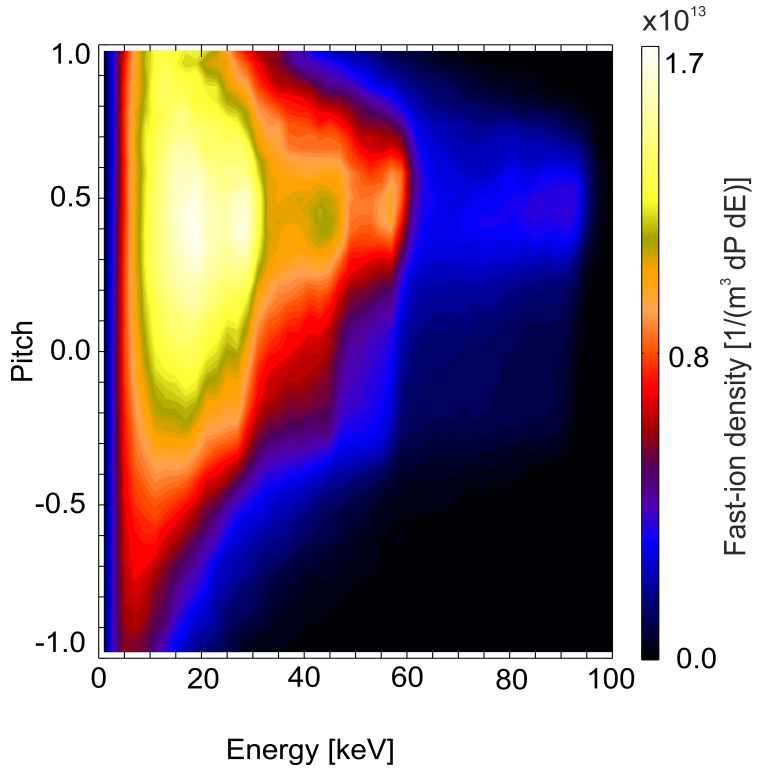

Figure 4.3: Volume averaged fast-ion distribution function used in this work. Slowing-down distribution function simulated with TRANSP. NBI beam 8 was active during the heating phase, as shown by the clear maximum centred at a pitch of 0,4

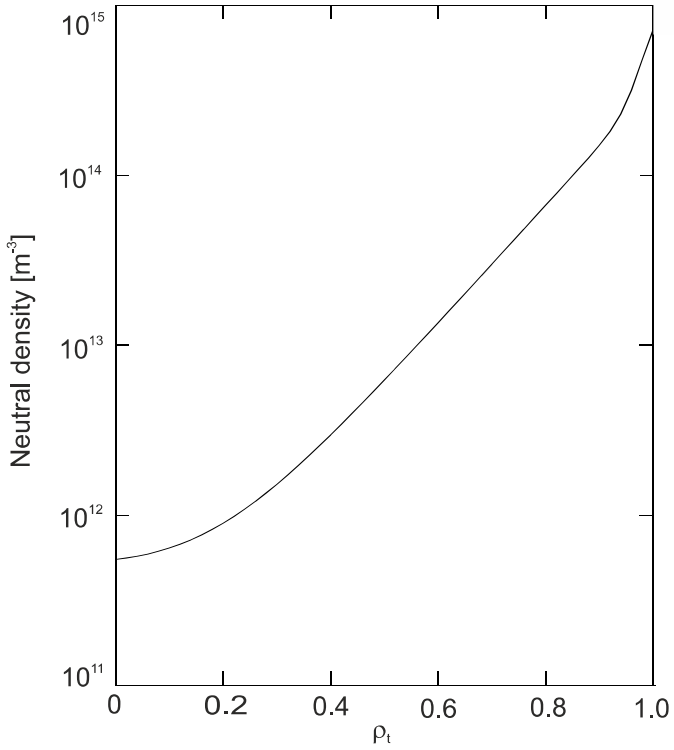

Figure 4.4: Passive neutral density profile used in the simulations.

4.1.2 Calculation of neutral densities: The collisional-radiative model

To compute the neutral density FIDASIM solves the collisional-radiative model, [21], that can be expressed shortly as:

$$\frac{dN_j}{dt} = \sum_k M_{jk} N_k \tag{4.2}$$

where N_j is the density of the neutral particles in the excited state j. FIDASIM assumes the population of each state of angular momentum l or other quantum number as a single population with their principal number n. The coefficients M_{jk} are the rates of the transition from the level k to the level j. In these rates all relevant physical processes that take part are included: ionization due to collisions with ions or electrons, charge-exchange reactions or collisions with impurities. It would be computationally very expensive to calculate the cross-sections for these rates during the program execution so all necessary cross-sections are loaded from external tables.

To calculate the deposition density of the NBI, according to the divergence of the beam and its geometry, FIDASIM calculates the initial flux of neutrals that are injected in one grid cell (the first one in the beam path). To be precise, it calculates the weight of each Monte Carlo marker that represents the neutral particles. With the velocity of the neutral and the grid size, the code calculates how much time the marker will spend on the cell. With this information, the rates, the cross-sections extracted from the tables and all plasma parameters taken from inputs, the collisional-radiative model is solved. The flux of neutrals going to the next cell is calculated and used as input for the solution of the model in that cell, then the process is repeated until the model is solved in every cell. FIDASIM stores the calculated neutral density in each cell but does not modify the fast-ion distributions adding the new ions generated during the CX reactions.

The halo neutral density is calculated in 'steps' that are called 'generations' as explained in [5]. The first generation is calculated by starting random markers in each cell of the grid according to the fast-ion distribution function and computing the CX reactions with the neutrals from the beam deposition. The second generation is computed taking into account the CX reactions between the neutrals from the first generation and the plasma ions. The following generations are computed in the same way as the second one but according to the neutral density of the previous generation. In each generation, the neutral density is smaller due to losses induced by ionizations processes so after a few generations, the changes are negligible. The computation is usually finished after less than ten iterations as no change in the neutral density is observed. The halo density is the sum of all densities from different generations.

4.1.3 Calculation of NPA signal

With all densities calculated, the analysis of the NPA signal starts. To calculate the NPA flux, FIDASIM integrates along the LOS:

$$\Phi(E_i) = \int F(E_i) n_n(\vec{r}) \sigma_{CX} V_{rel} \frac{\Delta\Omega}{4\pi} e^{-\lambda(l)} A dl \tag{4.3}$$

where $\Phi(E_i)$ represents the neutral flux, $F(E_i)$ the fast-ion distribution function, $n_n(\vec{r})\sigma_{CX}V_{rel}$ the CX rate (with $n_n(\vec{r})$ being the neutral density, σ_{CX} the cross-section of the CX reaction and V_{rel} the relative velocity between the neutral and the ion), $\frac{\Delta\Omega}{4\pi}A$ the geometric factor (with $\Delta\Omega$ being the solid angle subtended by the detector and A its area) and $e^{-\lambda(l)}$ the attenuation factor. The integral is computed by summing over all cells in which part of the LOS is contained. In each cell, random markers are launched, according to the fast-ion distribution function and only markers whose velocity vectors can hit the detector are kept. Then they are scaled by the CX rate and the geometric factor and multiplied by the

attenuation factor that depends upon the distance between the birth position and the detector.

FIDASIM stores all information about the calculated NPA signal in a binary file. For each marker it stores the impact point inside the head, the velocity, the weight, the type (whether it is active or passive signal) and the point where the neutral particles were born. All of this information is passed to INPASIM.

4.2 INPASIM

During this work, the INPASIM code for AUG has been developed. The code has two main parts, the characterization of the detector and the calculation of the signal. Both modules receive the geometry of the detector and the already mentioned physics information as an input.

The characterization module launches markers with random initial position on the pinhole and velocity (direction and modulus) fixed inside a range of values, and then tracks them until they collide, either with the pinhole or the scintillator. These markers with fixed energy, pitch and gyrophase[9] enable the mapping of the scintillator and the calculation of the resolution of the system. The signal module tracks all the FIDASIM markers until they collide with the collimator or scintillator.

The geometry setup is programmed in Matlab©. The script receives all parameters explained in chapter 3 as input and models the detector as a series of plain polygons. Each polygon is defined as a list of consecutive vertices. First, the plate is defined in an axis system with the x-axis parallel to the collimator, then a rotation and translation are applied to put the plate in the torus reference system. The data from each polygon is stored in a separate ASCII file.

9 The gyrophase is the angle that forms the velocity projection on the perpendicular plane (referred to magnetic field) with and arbitrary direction defined in that plane.

With all the geometry set up, the loading of the data begins. At this stage, all the information of the markers is loaded into a structure. Then, the signal calculation starts. The track algorithm is programmed in FORTRAN95 and the main structure of the code is shown in figure 4.5. One of the markers is chosen and as a first step, the code checks if it has been blocked at the pinhole; if the marker has entered, the code follows its straight trajectory (the markers represent neutral particles, hence no deflection due to the magnetic field exists) and checks if it collides with the collimator. If the marker did not experience a collision with the collimator, it calculates the collision point at the carbon slit. Then the ionization is simulated. Following SRIM simulations, non velocity scattering in the carbon foil is assumed and corrections to the energy of the markers are performed. No correction to the weight of the markers is applied because the ionization factor of the carbon foil has not been calculated. This ionization factor will depend on the density of the foil and the incident flux. At last, the helicoidal trajectory of the marker (now representing the ionized particles) and its intersection point with the scintillator is computed assuming that the particles are deuterium. The algorithm is repeated for every FIDASIM output marker. When all FIDASIM markers are computed, the code launches a series of markers with given velocity and tracks them as before. With these markers, the scintillator map is defined (see section 5.1)

The post-processing routines calculate the signal dividing the scintillator plate in a series of finite squares. The markers that hit the scintillator plate inside each of them are counted and plotted into a histogram. The first step of the post-processing mapping is the calculation of the same histogram with the mapping markers. The second is the computation of the resolution and the mapping following the criteria explained in section 5.1.

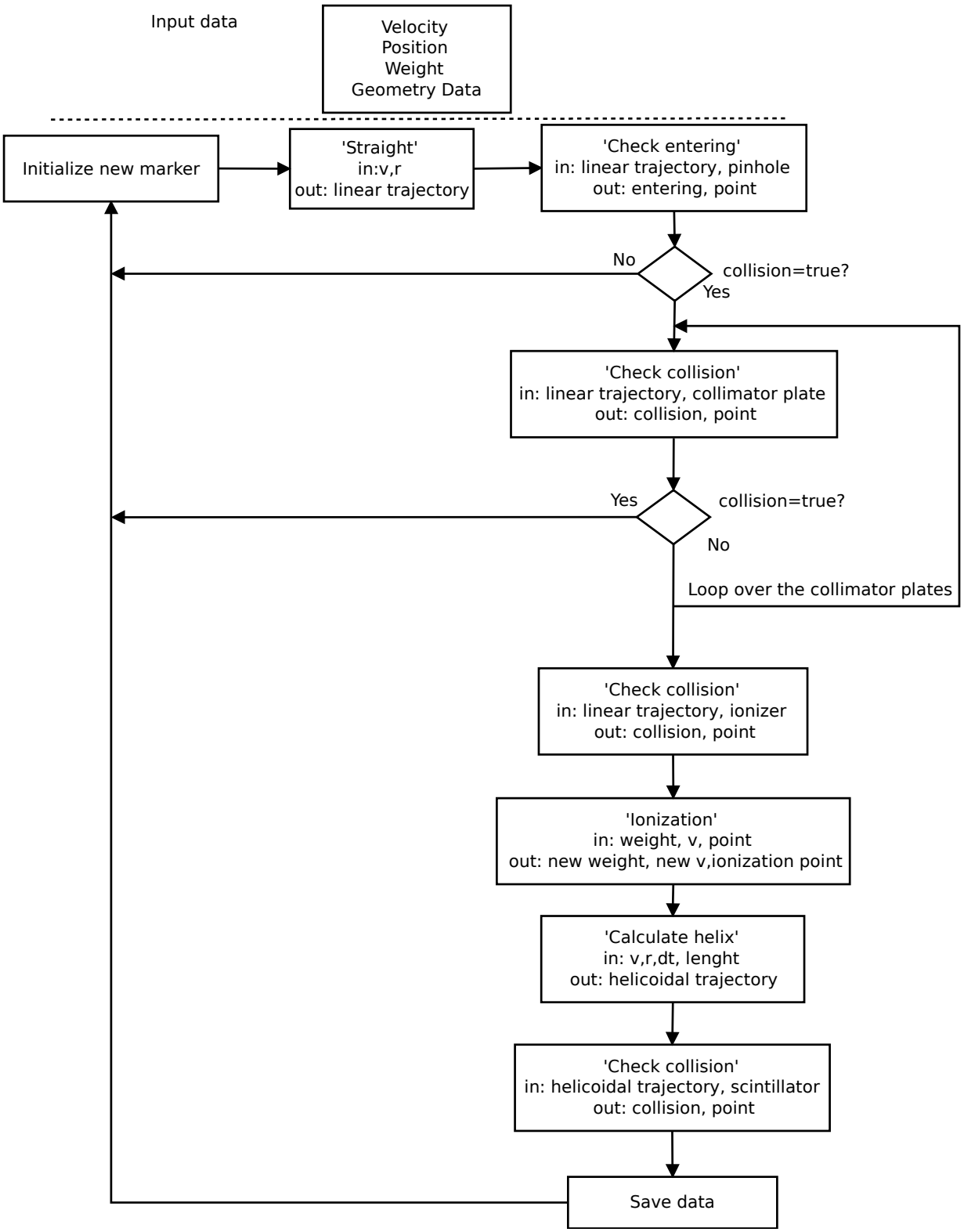

Figure 4.5: Flow diagram for the INPASIM code.

5 Results

In this chapter, the feasibility study for the INPA diagnostic, including the resolution study and the first calculated synthetic signal is presented.

5.1 Scintillator mapping and resolution study

The scintillator mapping has been performed based on the assumptions that the NBI beam 3 injects neutral particles following a perfect line.

A series of points have been chosen along the NBI beam 3 and particles have been randomly initialised at the pinhole with velocity direction given by the LOSs that intercept NBI beam 3 at these points and energy chosen inside the range of interest. As the collimator have been defined to have a perfect view of the NBI beam 3, none of these markers are collimated and the results are a series of uniformly distributed 'circles' in the scintillator (actually they are ellipses due to the orientation between the scintillator and the collimator). The representation of the result obtained can be seen in figure 5.1. There, the effect of the pinhole size on the resolution of the system can be seen. Basically each of these 'strike structures' is the image of the pinhole. If a smaller pinhole would be chosen, the resolution will improve; but in first approximation, the incoming flux is proportional to the pinhole area, so reducing the pinhole radius to half will reduce the signal by a factor of 4.

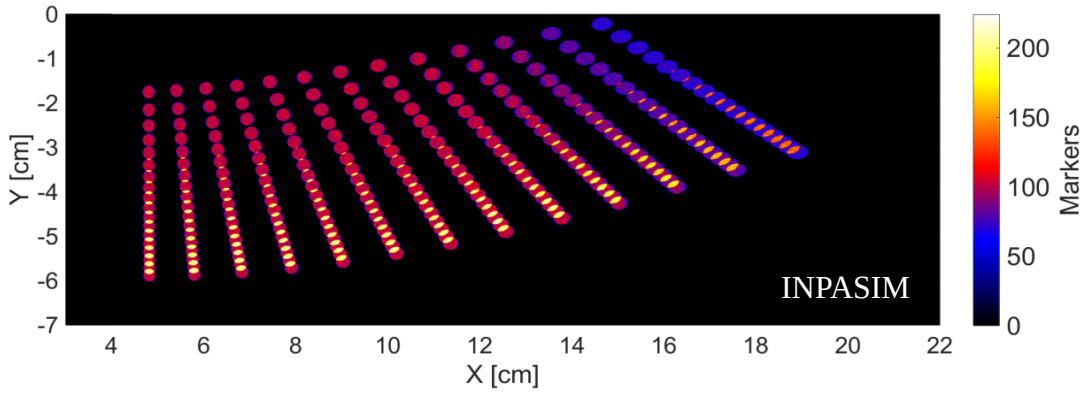

Figure 5.1: Strike structure recorded after launching the Monte Carlo markers to map the scintillator. Calculated with INPASIM.

The centre of mass of each strike structure has been calculated to define the points for the strike map. The calculated centroids can be seen in figure 5.2. In a zero order approach it can be assumed that the active component dominates the signal and if the halo is neglected all that active component will come directly from the interaction of the ions with the injected neutrals. So in this approximation, the signal from each LOS comes from the intersection point between the LOS and the NBI path. As the local pitch is determinate by the LOS too, there is a direct correspondence between the local pitch on the scintillator plate and the radial position in the plasma.

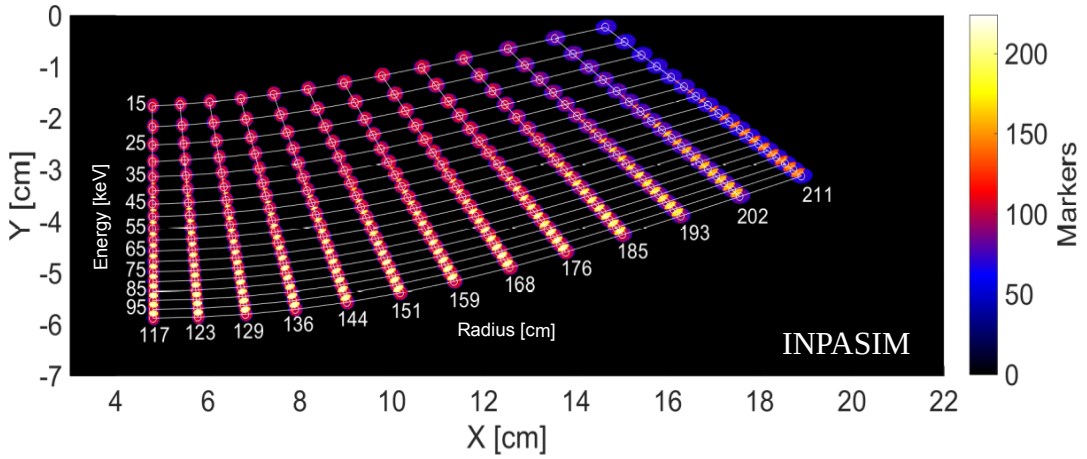

Figure 5.2: Strike map for the INPA scintillator calculated with INPASIM. Each 'vertical' line represents constant radius and each 'horizontal' line represent constant energy. Energy is expressed in keV and radius in cm.

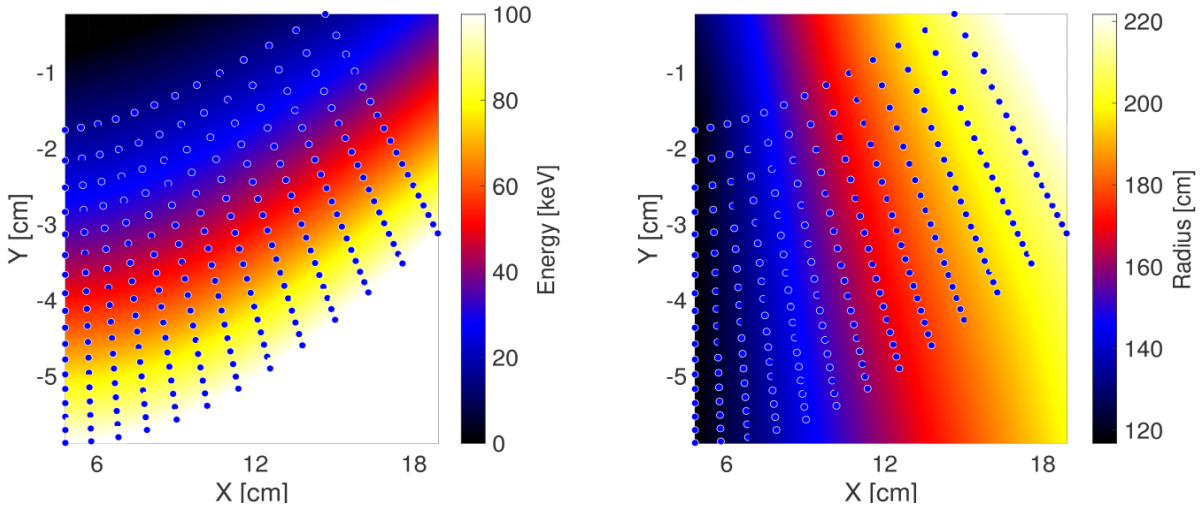

Figure 5.3: 2D splines that relate the scintillator coordinates with the energy (left figure) and pitch (right figure). Both fits have been done with Matlab©.

The resolution of the diagnostic has been defined as the 'radius' of the strike structures shown in figure 5.1. The radius has been chosen because it has been considered that if two circles have their centres separated slightly more than one radius, they can be identified. To calculate the extension of the strike structures in the energy-pitch space two 2D splines have been fit to the centroids, shown in figure 5.2, both splines can be seen in figure 5.3.

Based on these fits, the calculation of the resolution is straightforward. The resolutions in energy and pitch are shown in figures 5.4 and 5.5. As shown, the

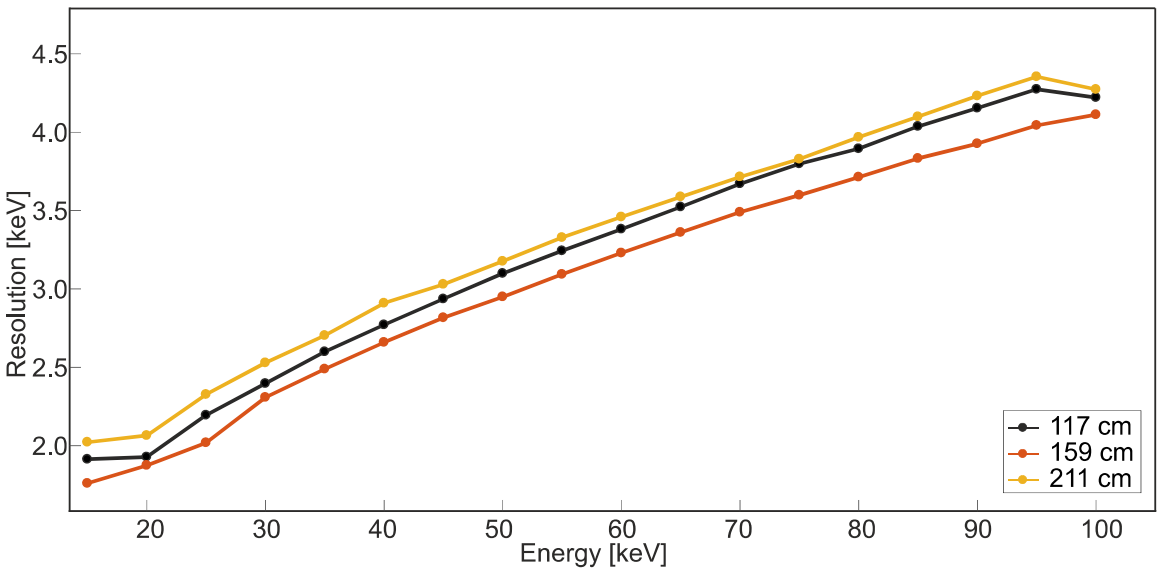

Figure 5.4: Energy resolution of the INPA for three selected values of the radial position.

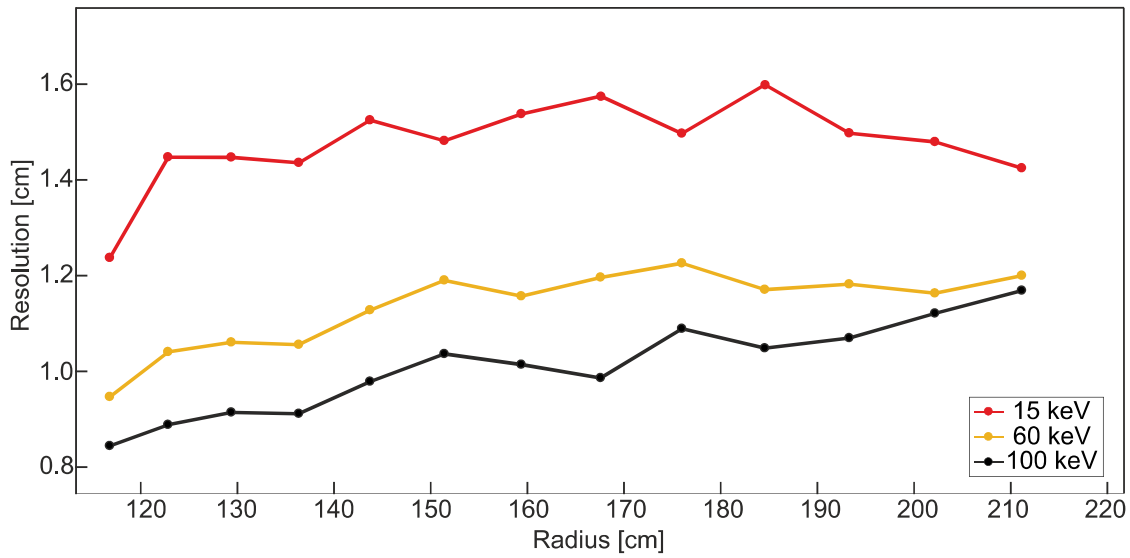

Figure 5.5: Radial resolution of the INPA for three selected values of energy.

system presents a good resolution, less than 5 keV in energy and less than 2 cm in radial direction. The former is in the range of DIII-D results (7.5 keV). The latter represent a lower limit. In reality other effects such as the finite size of the beam and the halo have to be taken into account to determine the upper limit of the radial resolution. In DIII-D set up, the radial resolution is 7 cm, similar resolution is expected for AUG set up.

Nonetheless, the resolution in energy (without taking into account the scintillator behaviour and the resolution of the cameras) can be determinate without any assumptions, as it only depends on the geometry of the system. To this end, random particles have been initialised at the pinhole as in the previous study but with no more restriction in their velocity direction that their pitch angles i.e. the gyrophases have been set randomly. With this, all possible trajectories that could be measured with the detector have been simulated. The strike structure is shown in figure 5.6. Instead of ellipses, now each strike structure is a rhomboid. The rhomboids appear due to the pinhole-collimator geometry, their width is determinate by the pinhole width and their height by the collimator height.

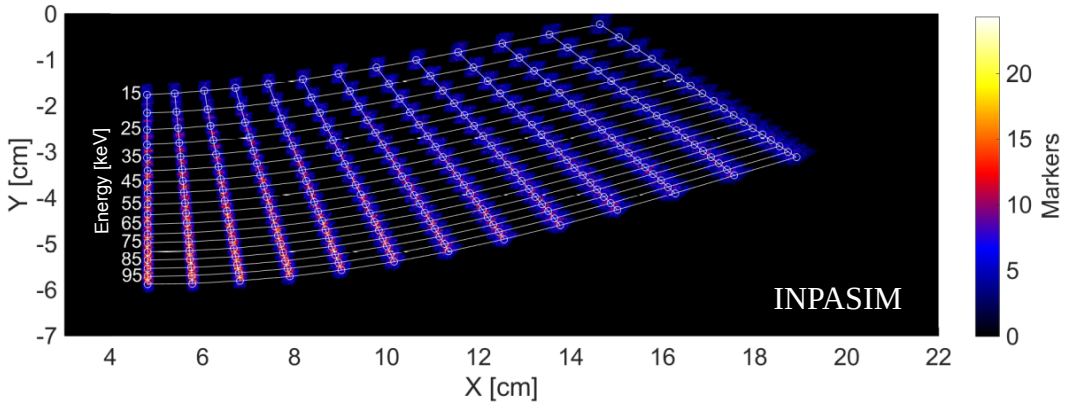

Figure 5.6: Strike structure recorded in the second energy resolution study.

As before, the centroid of each strike has been calculated and two 2D splines have been fit to them. In this case, the resolution in energy have been defined as half of the height of the rhomboid. The average of the energy resolution over all pitch values is given in figure 5.7. This more precise calculation for the energy resolution of the system shows that the diagnostic will have a good energy resolution, less than 6 keV. In the same figure, the energy resolution with different pinhole sizes is shown too. As shown, reducing the pinhole diameter improves the resolution of the diagnostic. Despite changing the pinhole diameter from 3 mm to 1.5 mm the resolution only improves in 1 keV and the signal will be reduced by a factor 4 (as mentioned earlier in this section, incident neutral flux is almost proportional to the area of the pinhole).

The collimator geometry will also affect the energy resolution of the system. The resolution calculated with different collimator heights (and a constant pinhole diameter of 3 mm) is shown in figure 5.8. Decreasing the height of the collimator improves the resolution but in this case a direct evaluation of how the signal will be affected can not be done. The calculated signal for different collimator heights is shown at the end of section 5.2.

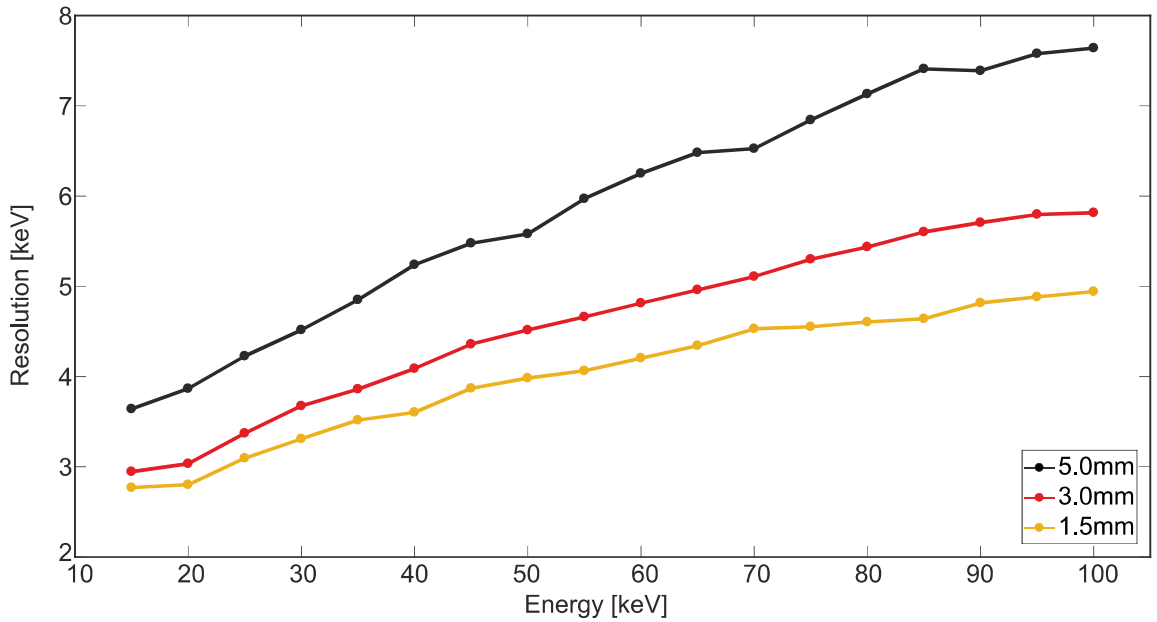

Figure 5.7: Energy resolution of the system for three pinhole diameters.

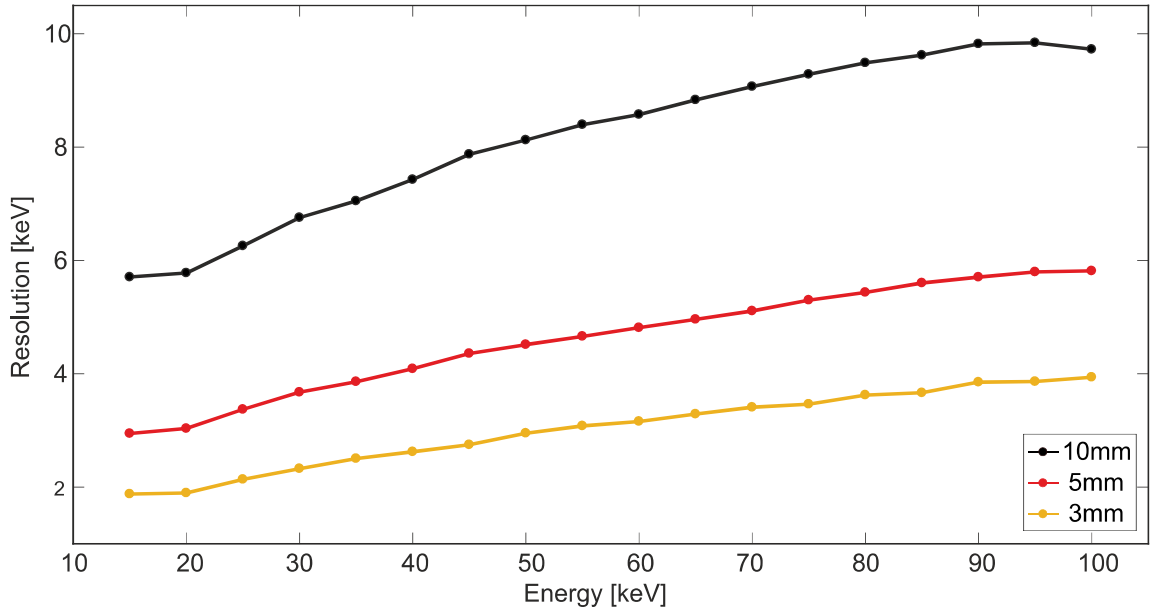

Figure 5.8: Energy resolution of the system for three collimator heights.

5.2 Study of the synthetic signal

Simulations have been carried out using the fast-ion distribution function calculated with TRANSP for shot #30585 (see figure 4.3). The simulated impacts on the scintillator plate are shown in figure 5.9. Note that no ionization factor has been applied, as mentioned in section 4.2, so the colour axis is qualitative. The

structure on the scintillator is not a direct representation of the fast-ion distribution function. This is because two important facts modulate the signal. First, as explained in section 2.5, the deposition profile of the NBI has a maximum near the plasma edge, so in that area there are more neutrals, thus the signal coming from that area is larger. Second, neutrals coming from the inner radius travel a larger distance through the plasma, so they suffer more attenuation (due to ionization processes). Due to these facts, the signal coming from the inner radius is two exponential factors smaller than the signal coming from the outer part of the torus. As shown in figure 3.5, the LOS that intercept NBI beam 3 at the larger radius explore higher values of pitch angle; looking now to figure 4.3 again, particles with high values of pitch have low values of energy. These two considerations can explain the recorded signal.

A direct separation of the active and passive signal can be done based on the simulations. These are shown in figures figures 5.10 and 5.11, respectively. Note that for the passive signal, the relation between pitch and radial position does not apply. All passive signal is coming from the plasma edge.

Looking at figures 5.10 and 5.11, the passive signal is globally two orders of magnitude smaller than the active one. Actually, the active signal and total signal are almost the same; but the passive signal is dominant in the pitch range corresponding to the inner radius, as was said this is due to the smaller active neutral density and the larger distance that the neutral must travel to reach the detector.

Figures 5.12 to 5.14 show the signal calculated with a collimator height of 3 mm. The structures of the recorded signal for both collimator heights are almost indistinguishable. Calculating the total flux, the narrower collimator configuration gives a signal that is only 12% less intense.

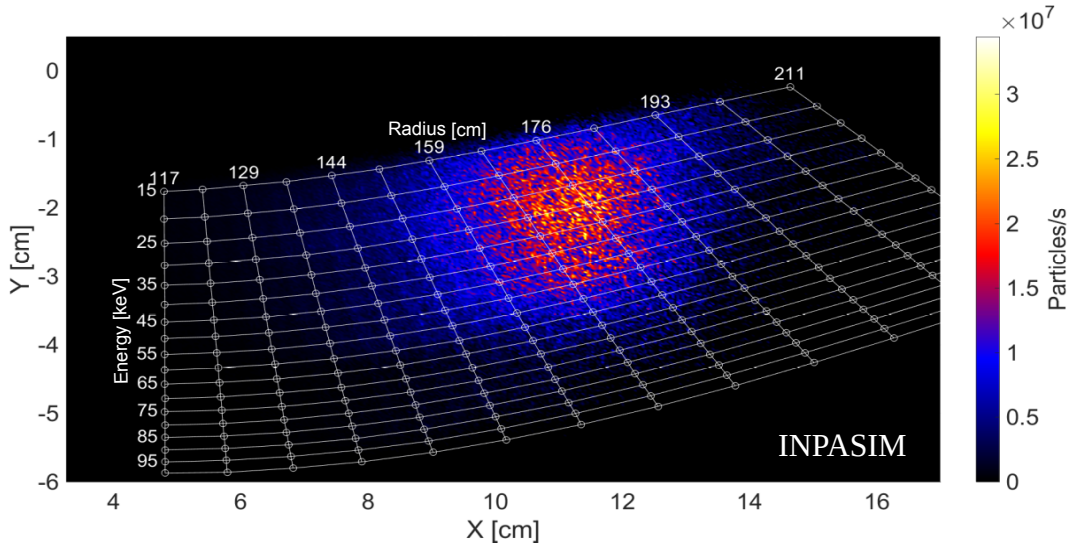

Figure 5.9: Synthetic signal of the INPA. The collimator height was set to 5 mm.

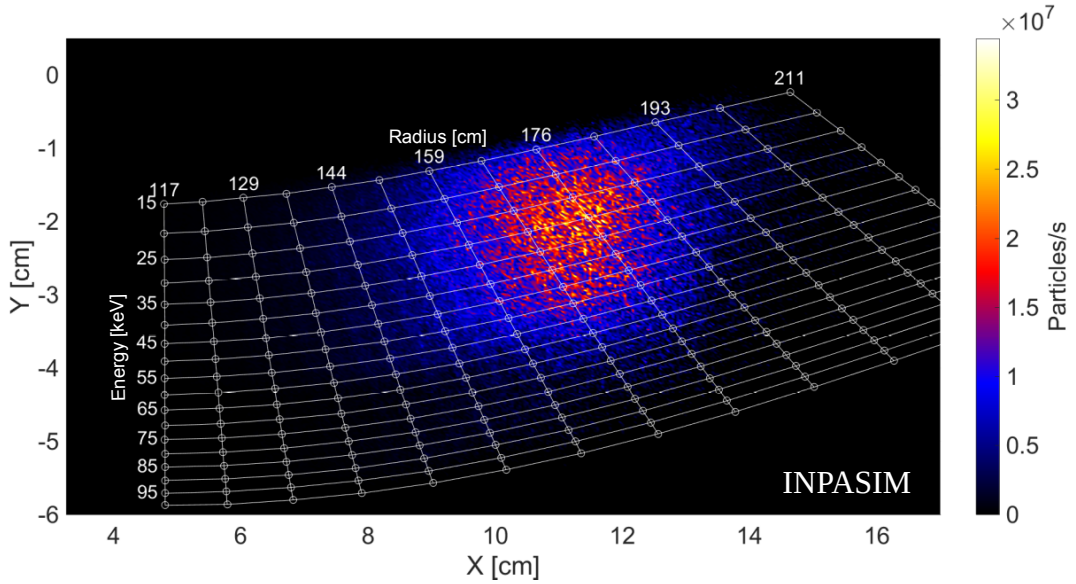

Figure 5.10: Synthetic active signal of the INPA. The collimator height was set to 5 mm.

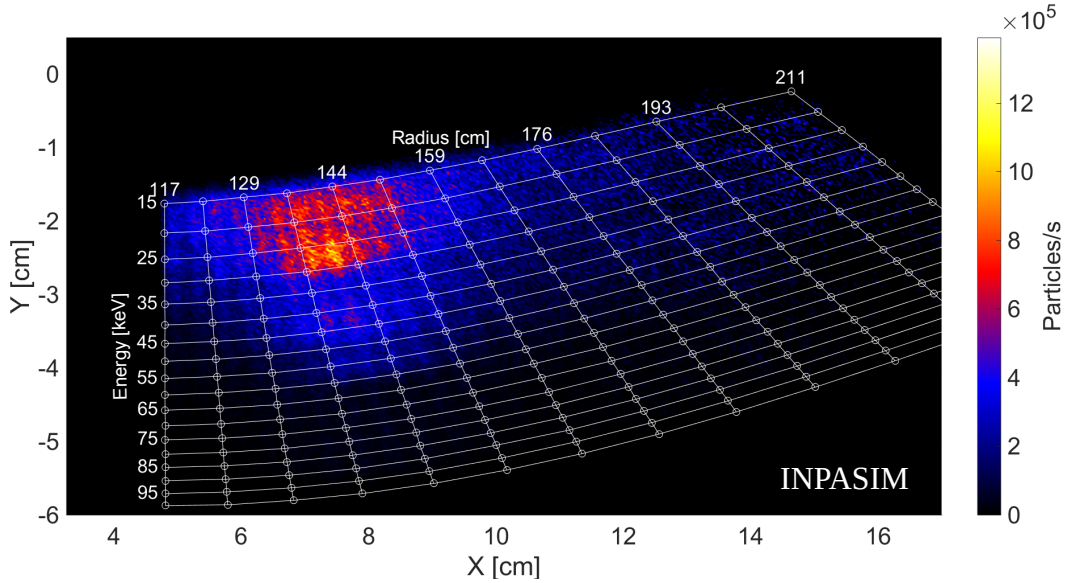

Figure 5.11: Synthetic passive signal. The collimator height was set to 5 mm. Note in the colour bar that the signal is two order of magnitudes smaller that the active component.

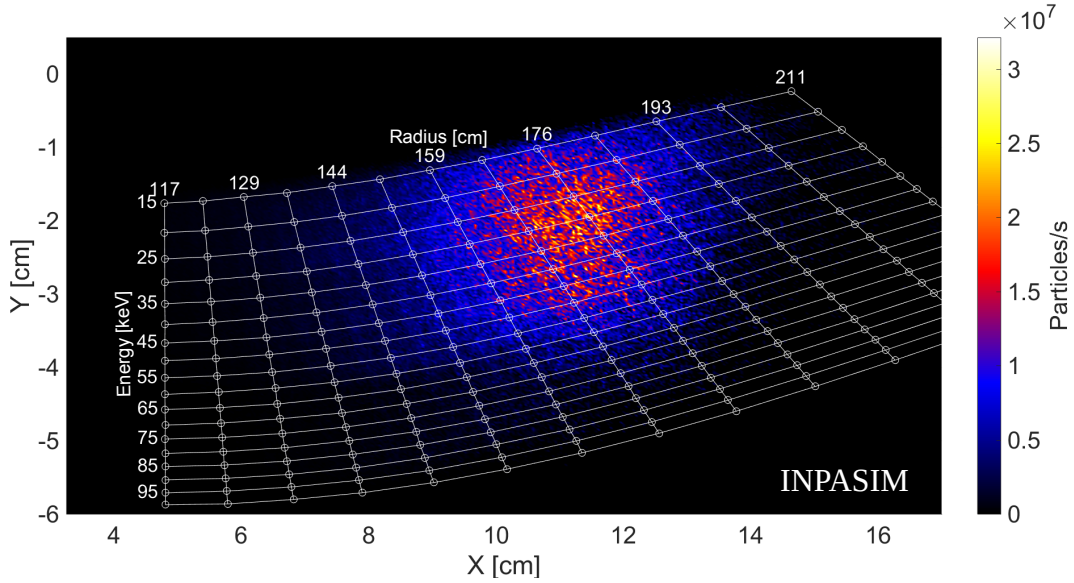

Figure 5.12: Synthetic signal of the INPA. The collimator height was set to 3 mm.

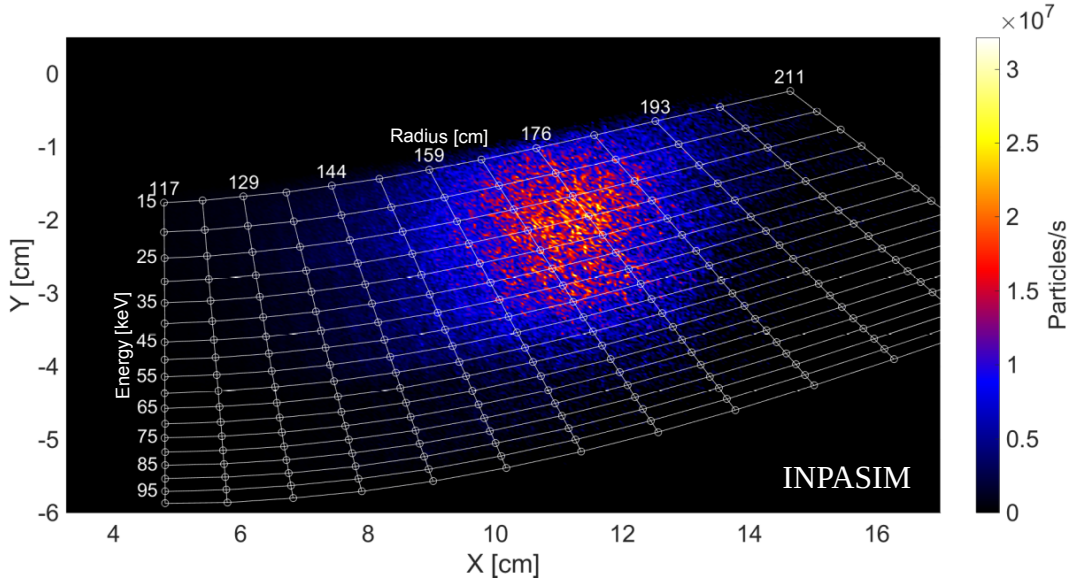

Figure 5.13: Synthetic active signal of the INPA. The collimator height was set to 3 mm.

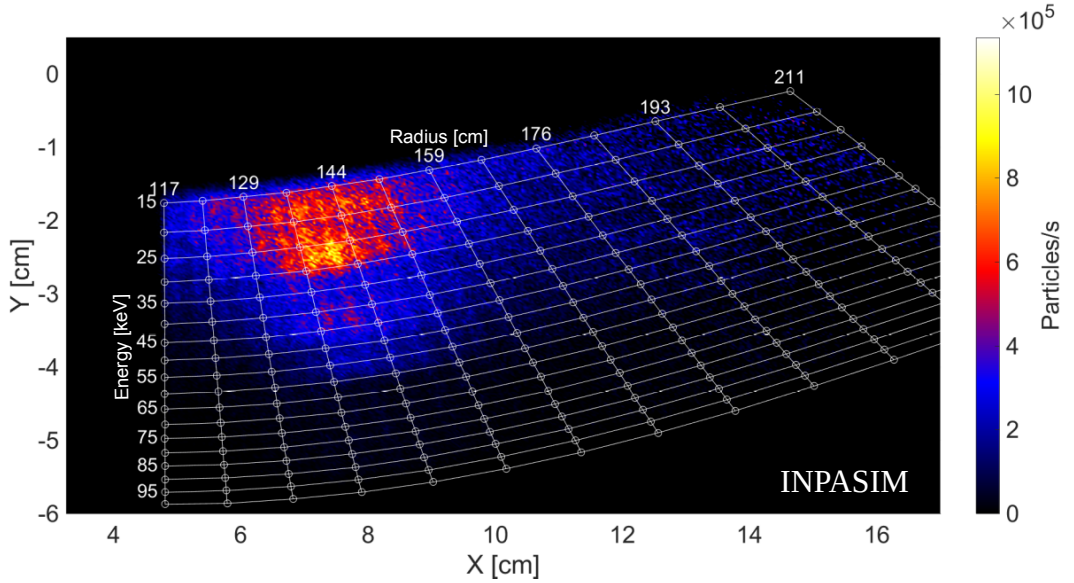

Figure 5.14: Synthetic passive signal of the INPA. The collimator height was set to 3 mm. Note in the colour bar that the signal is two order of magnitudes smaller that the active component.

6 Conclusions and future work

In this bachelor thesis, a feasibility study for a new imaging neutral particle analyser (INPA) diagnostic at ASDEX Upgrade was carried out. The advantage of INPA is that the radial profile of the confined fast-ions can be measured, as several lines of sight can be employed. INPASIM, a code to simulate the signal on the scintillator plate starting from the FIDASIM results, has been developed and tested successfully. During the study, various head positions and geometric configurations have been tested. The simulations show that high resolution in energy and radius (to first order, about 6 keV in energy; and as lower limit 2 cm in radius) and high level of signal can be obtained with an optimal selection of the geometry.

To develop a fully functional INPA, an optimization of the detector position to maximise the signal must be carried out; the mapping procedure needs to take into account the finite size of the neutral beam (about 20 cm at ASDEX Upgrade) and the ionization efficiency of the carbon foil must be measured. In addition, a weight function formalism needs to be implemented which will allow to deconvolve the strike structures on the scintillator plate.

Acknowledgements

I would like to thank Dr. Eleonora Viezzer, Dr. Manuel García and Dr. Juan Manuel Ayllón for giving me the opportunity to work in this project and answering with patience all my questions and in general to all PSFT group for its support. Also I would like to personally thank Dr. Mauricio Rodríguez for doing SRIM simulations and cheering me up during the last days of this work; and specially I would like to thank Joaquin Galdón, without his help and patience this work would have been impossible. Thank you all. Gracias

Bibliography

[1] J. A. Wesson, *Tokamaks*, 4º Edition. Oxford University Press, 2011.

[2] 'ASDEX Upgrade'. [Online]. Available: https://www.aug.ipp.mpg.de/wwwaug/. [Accessed: 22-Dec-2017].

[3] 'Tritium Breeding'. [Online]. Available: https://www.iter.org/mach/tritiumbreeding. [Accessed: 20-May-2018].

[4] P. A. Schneider *et al.*, 'A new compact solid-state neutral particle analyser at ASDEX Upgrade: Setup and physics modeling', *Rev. Sci. Instrum.*, vol. 86, no. 7, Jul. 2015.

[5] B. Geiger, 'Fast-ion transport studies using FIDA spectroscopy at the ASDEX Upgrade tokamak', PhD thesis, Ludwig Maximilians Universität München, 2012.

[6] X. Du, M. A. Van Zeeland, W. W. Heidbrink, and D. Su, 'Development and verification of a novel scintillator-based, imaging neutral particle analyzer in DIII-D tokamak', *Nucl. Fusion*, May 2018.

[7] F. F. Chen, *Plasma physics and controlled fusion*, 2º Edition. Springer, 2006.

[8] I. H. Hutchinson, *Principles of plasma diagnostics*, 2º Edition. Cambridge University Press, 2002.

[9] Luke Stagner, 'FIDASIM DIIID', 2018. [Online]. Available: https://d3denergetic.github.io/FIDASIM/. [Accessed: 11-Apr-2018].

[10] A. A. Rukhadze, A. F. Alexandrov, and L. S. Bogdankevich, *Principles of plasma electrodynamics*, 2º Edition. URSS, 2013.

[11] M. García-Muñoz, 'Fast response scintillator based detector for MHD induced energetic ion losses in ASDEX Upgrade', PhD thesis, Ludwig Maximilians Universität München, 2006.

[12] M. García-Muñoz, H. U. Fahrbach, and H. Zohm, 'Scintillator based detector for fast-ion losses induced by magnetohydrodynamic instabilities in the ASDEX upgrade tokamak', *Rev. Sci. Instrum.*, vol. 80, no. 5, 2009.

[13] M. Rodríguez, 'Calibración absoluta y aplicación de los detectores de pérdidas de iones rápidos basados en materiales centelleadores para dispositivos de fusión nuclear', PhD thesis, Universidad de Sevilla, 2017.

[14] M. García-Mũoz *et al.*, 'Characterization of scintillator screens for suprathermal ion detection in fusion devices', *J. Instrum.*, vol. 6, no. 4, 2011.

[15] M. Rodriguez-Ramos *et al.*, 'First absolute measurements of fast-ion losses in the ASDEX Upgrade tokamak', *Plasma Phys. Control. Fusion*, vol. 59, no. 10, 2017.

[16] J. Galdon-Quiroga *et al.*, 'Velocity-space sensitivity and tomography of scintillator-based fast-ion loss detectors', *Plasma Phys. Control. Fusion*, submitted, 2018.

[17] J. F. Rivero-Rodriguez *et al.*, 'A rotary and reciprocating scintillator based fast-ion loss detector for the MAST-U tokamak', *Rev. Sci. Instrum.*, accepted, 2018.

[18] R. Bartiromo *et al.*, 'Design and calibration of the JET neutral particle analyzer', *Rev. Sci. Instrum.*, vol. 58, p. 788, 1987.

[19] J. Ziegler, 'SRIM'. [Online]. Available: http://www.srim.org/. [Accessed: 15-Apr-2018].

[20] J. Galdon-Quiroga *et al.*, 'Velocity space resolved absolute measurement of fast ion losses induced by a tearing mode in the ASDEX Upgrade tokamak', *Nucl. Fusion*, vol. 58, no. 3, 2018.

[21] W. W. Heidbrink, D. Liu, Y. Luo, E. Ruskov, and B. Geiger, 'A code that simulates fast-ion Dα and neutral particle measurements', *Commun. Comput. Phys.*, vol. 10, no. 3, pp. 716–741, 2011.

[22] M. Sertoli, 'Local Effects of ECRH on Argon Transport at ASDEX Upgrade', PhD thesis, Ludwig Maximilians Universität München, 2010.

[23] E. Viezzer, T. Pütterich, R. Dux, A. Kallenbach, and the AUG Team, 'Investigation of passive edge emission in charge exchange spectra at the ASDEX Upgrade tokamak', *Plasma Phys. Control. Fusion*, vol. 53, no. 3, Mar. 2011.